ChemComm

Accepted Manuscript

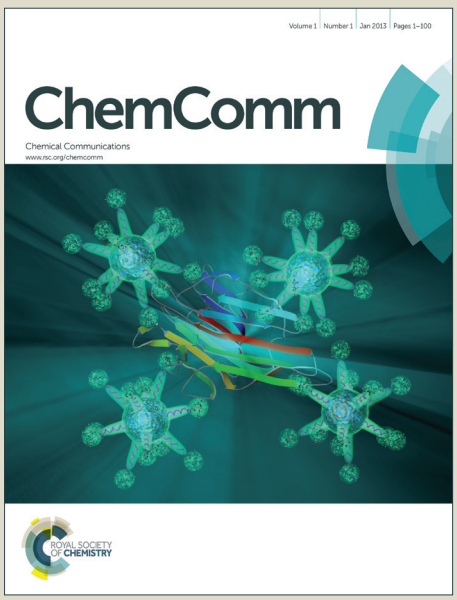

ROYAL SOCIETY OF CHEMISTRY

www.rsc.org/chemcomm

ARTICLE TYPE www.rsc.org/xxxxxx | XXXXXXXX

Electronic structures and electronic spectra of all-boron fullerene B_{40}

Rongxing He,[a,b] Xiao Cheng Zeng[b]**

Received (in XXX, XXX) XthXXXXXXXXX 200X, Accepted Xth XXXXXXXXX 200X
First published on the web Xth XXXXXXXXX 200X
DOI: 10.1039/b000000x

This study is motivated by the recent discovery of the first all-boron fullerene analogue, B_{40} cluster with D_{2d} point-group symmetry, dubbed borospherene (*Nat. Chem.* 2014, 6, 727). Insight into the electronic structures and spectral properties of B_{40} is timely and important to understand borospherene and the transition from open-ended plate or ribbon-like structures to hollow-cage structure at B_{40}. Optimized geometries of borospherene B_{40} for both ground state and the first excited state allow us to compute spectral properties including UV-vis absorption, infrared (IR) and Raman spectra. Highly resolved absorption and emission spectra are obtained, for the first time, for any fullerenes at the time-dependent density-functional theory (TD-DFT) level within the Franck-Condon approximation and including the Herzberg-Teller effect. Assigned vibrational modes in absorption and emission spectra are readily compared with future spectroscopy measurements to distinguish the hollow-cage structure of D_{2d}-B_{40} from other quasi-planar boron structures.

Since the discovery of the buckminsterfullerene C_{60}[1], carbon-fullerene-like elemental hollow-cage structures have been highly sought, particularly for nonmetal elements next to carbon in the periodic table. To date, it has been established that silicon, a nearest-neighbor of C in the periodic table, cannot form carbon fullerene-like structures, but can exhibit endohedral-like fullerene structures with uneven surface beyond the size of 30-atom clusters.[2] Boron, another nearest-neighbor of C in the periodic table, was initially predicted to form a fullerene-like structure at the cluster size B_{80}.[3] But later computational studies showed that the B_{80} fullerene is a high-energy isomer. Previous experimental and theoretical studies also indicated that all-boron fullerene analogue cannot be formed for small to medium-sized boron clusters up to the cluster size of 36.[4,5] Very recently, a fascinating all-boron fullerene structure, B_{40} hollow-cage (Figure 1a), was uncovered through a joint experimental/theoretical study.[5] Unlike C_{60} fullerene which is composed of pentagons and hexagons and has the I_h group symmetry[6], the box-like B_{40} fullerene is composed of hexagons and heptagons and has the D_{2d} group symmetry. As such, the electronic structures and spectral features of B_{40} are expected to be very different from those of C_{60}.[7] In light of the fact that this D_{2d}-B_{40} structure has not been directly imaged or observed in the laboratory[5], it is important to compute electronic and spectral properties of the B_{40} fullerene or borospherene for comparison with future spectroscopy measurements. In this communication, we present the first highly-resolved $S_0 \leftrightarrow S_1$ optical absorption and fluorescence spectra of B_{40}, on basis of the Frank-Condon (FC) approximation with including the Herzberg-Teller (HT) effect (intensity borrowing)[8]. Computed IR and Raman spectra are also presented. Although it is still a challenge to precisely simulate highly resolved electronic spectra because of the difficulty to optimize excited states, the present method has proven to be reliable as it has been benchmark tested in our previous studies.[9,10]

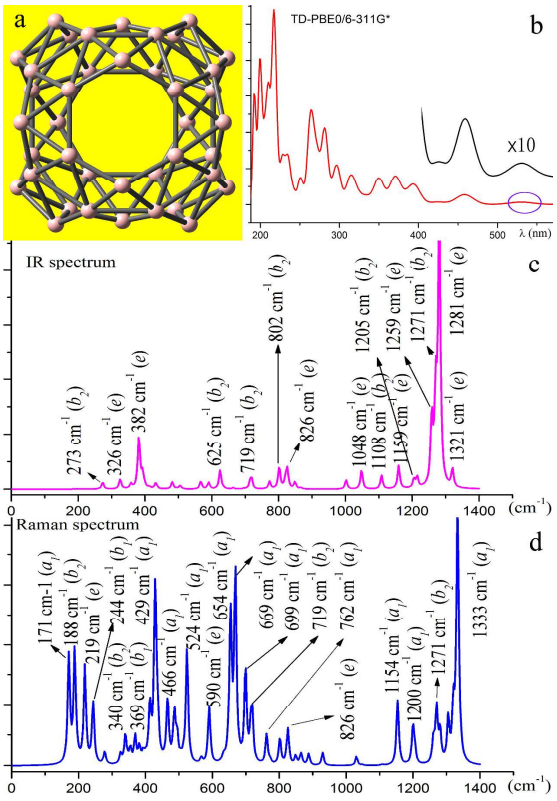

Figure 1. Borospherene B_{40} structure (a), and the computed optical spectra: (b) vertical absorption, (c) IR, and (d) Raman.

According to character table of D_{2d} point-group, the irreducible representations for the 114 vibrational normal modes of B_{40} are given as: $\Gamma_{tot} = 16a_1 + 13a_2 + 14b_1 + 15b_2 + 28e$. The corresponding vibrational frequencies are predicted using the PBE0 and BHandLYP functionals with 6-311G* and 6-31G* basis sets, and the results are given in Table S1 in the electronic supplementary information (ESI)†. Calculated vertical absorption (UV-vis) spectrum (Figure 1b) indicates that the strong dipole allowed transitions should take place in the region below the wavelength 400 nm. The lowest singlet excited state (S_1), assigned as B_2 symmetry, is weakly allowed absorption at ~532 nm with very small oscillator strength (denoted by an oval in

Figure 1b). The highest occupied molecular orbital (HOMO, π orbital) and the lowest unoccupied molecular orbital (LUMO, π* orbital) of the ground state, computed based on the PBE0/6-31G* level, are shown in ESI Figure S1. The computed results indicate that the excitation from $S_0(^1A_1)$ to $S_1(^1B_2)$ is the HOMO→LUMO transition with the vertical transition energy of 2.32 eV (see Table 1). Hence, S_1 state has the characteristic of π→π* transition. Note that in ref. 5, the computed ground-state adiabatic detachment energy of B_{40}^- anion is 2.39 eV, which is in good agreement with the present HOMO-LUMO excitation of 2.32 eV.

Compared with I_h-C_{60} fullerene for which only 14 normal modes are IR ($4t_{1u}$) or Raman ($2a_g + 8h_g$) active[11], the number of IR or Raman active modes of the borospherene B_{40} are significantly larger. Indeed, as shown in Figure 1c and 1d, the computed IR and Raman spectra of B_{40} do display numerous active absorption peaks. Detailed IR and Raman peak positions, intensities and assignments are given in ESI Table S2. The D_{2d}-B_{40} encompasses 43 IR ($15b_2 + 28e$) and 73 Raman ($16a_1 + 14b_1 + 15b_2 + 28e$) active modes. However, intensities of most IR and Raman active modes are very weak. Especially for the IR spectrum, only modes ν_{22} (382 cm^{-1}), ν_{104} (1259 cm^{-1}), ν_{107} (1271 cm^{-1}) and ν_{108} (1281 cm^{-1}) exhibit strong vibration. Note that ν_{22}, ν_{104} and ν_{108} are two-fold degenerate normal modes with e symmetry, both being the main IR active modes according to our computation. Likewise, those modes with a_1 symmetry contribute mainly to the Raman spectrum. Note also that in the study of carbon nanotubes, the so-called "radial breathing mode" (RBM) is used to identify the hollow structures.[12] Here we report the RMB frequency of B_{40} with hollow structure is about 171 cm^{-1} (at PBE0/6-311G* level).

Table 1. Computed vertical transition energy (ΔE), adiabatic energy (E^{00}) and oscillator strengths (f) of the first five excited states of borospherene B_{40} (at PBE0/6-311G* level).

State	*configuration*	ΔE^a	f	$E^{00\,a}$
1^1B_2	HOMO → LUMO (70%)	2.32	0.006	1.96 [b]
1^1B_1	HOMO-1 → LUMO (70%)	2.34	0.000	
1^1E	HOMO-3 → LUMO (69%) HOMO → LUMO+1 (13%)	2.40	0.001	
2^1E	HOMO-2 → LUMO (69%) HOMO-1 → LUMO+2 (13%)	2.40	0.001	
1^1A_2	HOMO-4 → LUMO (69%)	2.51	0.000	

[a] Unit is in eV. [b] The PBE0/6-31g* level is used.

Next, we present the electronic spectra of borospherene B_{40}. The FC approximation is most satisfactory for description of vibrational transition with large oscillator strength, giving rise to the so-called FC spectrum. For weak and forbidden transition, the HT effect is important to give full and rich vibrational structures.[10] Thus, using the method published previously[9,10], we obtain highly-resolved electronic absorption and emission spectra of B_{40} with including the HT effect. We have assigned most of the involved vibrational normal modes (the results are displayed in Figure 2, ESI Figure S2 and Table S3). Note that the band origin is set at 15808 cm^{-1} (1.96 eV), which is the computed adiabatic energy gap between S_0 and S_1 (Table 1). The assignment is expected to offer a guideline for future B_{40} isomeric structure identification. The simulated spectra which include both FC and HT contributions are denoted as FCHT. To investigate the HT effect separately, the spectra involving only the HT contribution are also plotted (see ESI Figures S2b and S2e).

The harmonic approximation is used to simulate FC spectrum due to the difference between vibrational frequencies of S_0 and S_1 states is small for every totally symmetric (a_1 under D_{2d} point group) normal mode (the largest difference is about 20 cm^{-1} in the present situation, see ESI Table S4). The vertical transition results show that the $S_1 \leftarrow S_0$ absorption spectrum of B_{40} is very weak in the visible region with oscillator strength of 0.006 (Table 1). ESI Figure S2a shows that the FC spectral profile is dominated by the 0-0 transition. This suggests only small displacement of the position of the minimum on the potential energy surface between ground- and excited-states is generated[9], which is confirmed by the small Huang-Rhys factors of totally symmetric normal modes (see ESI Table S5). Our computation also suggests that the FC spectral profile of borosepherene B_{40} is primarily described by the FC progression in terms of nine totally symmetric normal modes and their combination. The computed frequencies of these nine modes (ν_2, ν_{22}, ν_{35}, ν_{37}, ν_{38}, ν_{49}, ν_{63}, ν_{102} and ν_{114}) are 172, 339, 432, 443, 455, 518, 660, 1181 and 1316 cm^{-1}, respectively (note that in the simulated absorption spectrum, frequencies of S_1 state are used, while in the emission spectrum frequencies of S_0 are adopted). Among FC active modes, ν_2, ν_{22}, ν_{37}, ν_{49}, ν_{63} and ν_{102} are the longest progression-forming modes, and modes ν_{35}, ν_{38} and ν_{114} have little contribution to the FC absorption spectrum. The relative intensities of some combined peaks, such as 49^122^1, 102^122^1 and 63^149^2, are significant and cannot be ignored. It is interesting to note that in the FC absorption spectrum, the most intensive vibrational band is from mode ν_{49}, and its relative intensity (25.62) is about one-fourth of the 0-0 transition (see ESI Table S3). This will be compared with the FCHT absorption spectrum.

Figure 2a displays the simulated FCHT spectral profile of B_{40}, where the tentative assignments of major vibrational transitions are presented (detailed assignments are given in ESI Figure S3). The strong impact of HT contribution to the spectrum could be easily seen by comparing the profiles of the FC and FCHT spectra (see ESI Figures S2a-S2c). Compared with the FC absorption spectrum, a large number of vibrational lines with strong intensity appear in the FCHT spectrum, as labeled in red. Within the region of 0-1500 cm^{-1} (the origin of 0-0 line is set as 0), one dominant congestion is shaped along twelve fundamental modes 2^1, 12^1 (261 cm^{-1}), 22^1, 27^1 (393 cm^{-1}), 31^1 (398 cm^{-1}), 38^1, 49^1, 60^1 (656 cm^{-1}), 99^1 (1148 cm^{-1}), 102^1, 111^1 (1283 cm^{-1}), and 114^1 (their relative intensities are listed in ESI Table S3). Among these modes, six non-totally symmetric normal modes, ν_{12}, ν_{27}, ν_{31}, ν_{60}, ν_{99} and ν_{111}, make great contribution to the FCHT spectrum (see ESI Figure S2b). Especially, modes ν_{27} and ν_{60} become the most intensive peaks in the FCHT spectrum, which is completely different from the FC spectrum. In addition, the HT active modes also significantly change the spectral profile in high

frequency region by the combined bands, such as $114^{1}12^{1}$ (ν_{114} + ν_{12} = 1577 cm^{-1}), $102^{1}60^{1}$ (ν_{102} + ν_{60} = 1837 cm^{-1}), etc.

The simulated $S_1 \rightarrow S_0$ emission spectra of borospherene B_{40} and the assignment are displayed in Figure 2b (For convenience, the FC and HT spectra are given in ESI Figure S2). Similar to the FC absorption, the 0-0 transition of the FC emission spectrum is also found to carry most of the FC intensity. Four active FC totally symmetric normal modes, ν_1 (171 cm^{-1}), ν_{17} (354 cm^{-1}), ν_{49} (524 cm^{-1}) and ν_{99} (1200 cm^{-1}), have the largest Huang-Rhys factors (see ESI Table S5), indicating that they are the primary progression forming modes. From ESI Figure S2e, one can see that the HT contribution also has a large effect to the emission spectral profile. In the FCHT emission spectrum, a primarily difference is seen in the range of 1250~1300 cm^{-1}, where the superposition of three non-totally symmetric normal modes, ν_{104}, ν_{107} and ν_{108}, leads to a strong transition with relative intensity comparable to that of mode ν_{49}. Briefly, the basic feature of FCHT emission spectrum of B_{40} is described by those bands at 171, 354, 382, 429, 437, 524, 654, 1200, 1271 and 1281 cm^{-1}, which are tentatively assigned as modes ν_1, ν_{17}, ν_{22}, ν_{31}, ν_{35}, ν_{49}, ν_{60}, ν_{99}, ν_{107} and ν_{108}. Moreover, one can find that the mirror symmetry between the FC absorption and emission spectra is almost retained, whereas mirror symmetry breakdown (MSB) can be observed between the FCHT absorption and emission spectra. Based on the analyses above, we therefore attribute the MSB to the HT effect.

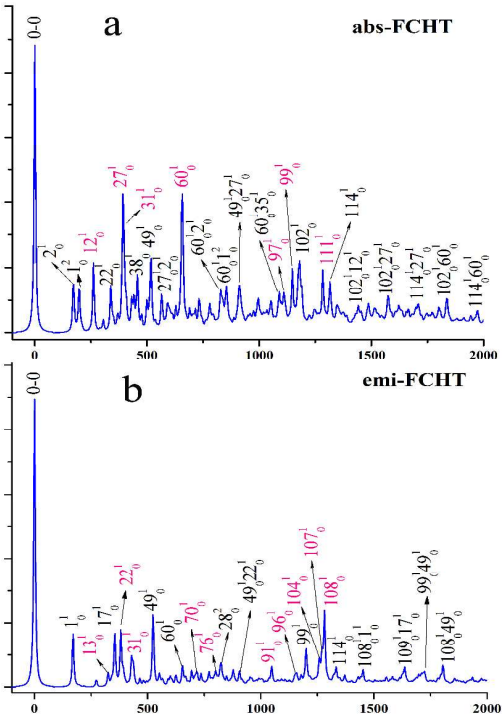

Figure 2. Simulated well-resolved absorption (a) and emission (b) spectra of borospherene B_{40} within a range of 2000 cm^{-1} (the 0-0 line is set to zero).

In summary, we have investigated electronic and spectral properties of the hollow-cage structure B_{40}. The computed vertical absorption spectrum suggests that the $S_0(^1A_1) \rightarrow S_1(^1B_2)$ is a weakly allowed absorption with $\pi\pi^*$ feature. The computed IR and Raman spectra suggest that there are 43 IR ($15b_2$ + $28e$) and 73 Raman ($16a_1$ + $14b_1$ + $15b_2$ + $28e$) active modes, but only a few of them have strong absorption. More importantly, the well-resolved $S_0(^1A_1) \rightarrow S_1(^1B_2)$ absorption and emission spectra of B_{40} are simulated, where the vibrational assignments are made tentatively. The HT effect has great influence on the simulated electronic spectra, which produces a richer vibrational structure and leads to the mirror symmetry breakdown between the absorption and emission spectra. The present results can be used, when compared with future spectroscopy measurements, to distinguish the hollow-cage structure of D_{2d}-B_{40} from other quasi-planar structures (as shown in ESI Table S6 and Figure S4, one can see that the IR and Raman spectra of the plate-like isomer B_{40}[5] are markedly different from those of the hollow-cage B_{40} isomer).[4a, 4b, 4c, 5, 13] The obtained optical spectra will be helpful not only for identifying the borospherene B_{40} among its quasi-planar isomers, but also for analyzing main features of the electronic transitions in the weakly allowed $S_0(^1A_1) \leftrightarrow S_1(^1B_2)$ absorption and fluorescence spectra. Knowledge on the spectral properties should be useful for the understanding and the transition from open-ended quasi-planar structures to the hollow-cage structure at B_{38} and B_{40}.[14,5]

RXH acknowledges the financial support from Natural Science Foundation of China (21173169), Chongqing Municipal Natural Science Foundation (cstc2013jcyjA90015) and the Fundamental Research Funds for the Central Universities (No. XDJK2013A008). XCZ is supported by NSF (Grant No. DMR-1420645), and UNL Holland Computing Centre, and a grant from USTC for (1000 Talent Plan) summer research.

[a] *Key Laboratory of Luminescence and Real-Time Analytical chemistry (Southwest University), Ministry of Education, College of Chemistry and Chemical Engineering, Southwest University, Chongqing 400715, China. E-mail: herx@swu.edu.cn*
[b] *Department of Chemistry, University of Nebraska-Lincoln, Lincoln, Nebraska, 68588, USA. E-mail: xzeng1@unl.edu*

†Electronic supplementary information (ESI) available: Computational details, vibrational frequencies of S_0 and S_1 states, spectral assignments and cartesian coordinates of all optimized structures of B_{40}.

Notes and references

1 H. W. Kroto, J. R. Heath, S. C. O'Brien, R. F. Curl and R. E. Smalley, *Nature*, 1985, **318**, 162.
2 (a) J. Bai, L.-F. Cui, J. Wang, S. Yoo, X. Li, J. Jellinek, C. Koehler, T. Frauenheim, L.-S. Wang and X. C. Zeng, *J. Phys. Chem. A*, 2005, **110**, 908; (b) S. Yoo, J. Zhao, J. Wang and X. C. Zeng, *J. Am. Chem. Soc.*, 2004, **126**, 13845.
3 (a) N. Gonzalez Szwacki, A. Sadrzadeh and B. Yakobson, *Phys. Rev. Lett.*, 2007, **98**; (b) H. Li, N. Shao, B. Shang, L.-F. Yuan, J. Yang and X. C. Zeng, *Chem. Commun.*, 2010, **46**, 3878; (c) J. Zhao, L. Wang, F. Li and Z. Chen, *J. Phys. Chem. A*, 2010, **114**, 9969.
4 (a) W. An, S. Bulusu, Y. Gao and X. C. Zeng, *J Chem Phys*, 2006, **124**, 154310; (b) B. Kiran, S. Bulusu, H. J. Zhai, S. Yoo, X. C. Zeng and L. S. Wang, *Proc. Natl. Acad. Sci. USA*, 2005, **102**, 961; (c) Z. A. Piazza, H. S. Hu, W. L. Li, Y. F. Zhao, J. Li and L. S. Wang, *Nat. Commun.*, 2014, **5**, 3113; (d) A. P. Sergeeva, Z. A. Piazza, C. Romanescu, W. L. Li, A. I. Boldyrev and L. S. Wang, *J. Am. Chem. Soc.*, 2012, **134**,

18065; (e) H. J. Zhai, A. N. Alexandrova, K. A. Birch, A. I. Boldyrev and L. S. Wang, *Angew. Chem. Int. Ed.*, 2003, **42**, 6004; (f) H. J. Zhai, B. Kiran, J. Li and L. S. Wang, *Nat. Maters.*, 2003, **2**, 827.

5 H. J. Zhai, Y. F. Zhao, W. L. Li, Q. Chen, H. Bai, H. S. Hu, Z. A. Piazza, W. J. Tian, H. G. Lu, Y. B. Wu, Y. W. Mu, G. F. Wei, Z. P. Liu, J. Li, S. D. Li and L. S. Wang, *Nat. Chem.*, 2014, **6**, 727.

6 V. Schettino, M. Pagliai, L. Ciabini and G. Cardini, *J. Phys. Chem. A*, 2001, **105**, 11192.

7 A. Sassara, G. Zerza, M. Chergui, F. Negri and G. Orlandi, *J. Chem. Phys.*, 1997, **107**, 8731.

8 F. Santoro, A. Lami, R. Improta, J. Bloino and V. Barone, *J Chem Phys*, 2008, **128**, 224311.

9 M. Guo, R. He, Y. Dai, W. Shen, M. Li, C. Zhu and S. H. Lin, *J Chem Phys*, 2012, **136**, 144313.

10 P. Yang, D. Qi, G. You, W. Shen, M. Li and R. He, *J Chem Phys*, 2014, **141**, 124304.

11 D. S. Bethune, G. Meijer, W. C. Tang, H. J. Rosen, W. G. Golden, H. Seki, C. A. Brown and M. S. de Vries, *Chem. Phys. Lett.*, 1991, **179**, 181.

12 A. K. Singh, A. Sadrzadeh and B. I. Yakobson, *Nano Lett.*, 2008, **8**, 1314.

13 (a) W. Huang, A. P. Sergeeva, H. J. Zhai, B. B. Averkiev, L. S. Wang and A. I. Boldyrev, *Nature chemistry*, 2010, **2**, 202; (b) I. A. Popov, Z. A. Piazza, W. L. Li, L. S. Wang and A. I. Boldyrev, *J Chem Phys*, 2013, **139**, 144307.

14 J. Lv, Y. Wang, L. Zhu and Y. Ma, *Nanoscale*, 2014, **6**, 11692.